Workflow and Lab-Scale Demonstrator of an on-substrate 3D-Printed Window Frame

Adam Pajonk[1,2*], Alessandra Luna-Navarro[1], Ulrich Blum[2], Ulrich Knaack[1]

* Corresponding author: Corresponding author: A.M.Pajonk@tudelft.nl
1 Delft University of Technology, Faculty of Architecture and the Built Environment, Department of Architectural Engineering + Technology, Architectural Facades & Products Research Group, Netherlands
2 Muenster University of Applied Sciences, Faculty of Architecture, Department of Digital Design and Construction, Germany

Abstract
Additive Manufacturing offers significant potential in construction by directly converting digital designs into physical objects. However, this potential is constrained by the separated fabrication approach–components are printed away from their final location and later installed. Inherent to most AM processes, it disrupts automation and adds complexity to the construction process. This study demonstrates a laboratory on-substrate workflow that prints directly onto the receiving substructure. A comprehensive workflow was developed, integrating digital design, slicing, and robotic on-substrate Additive Manufacturing to address challenges such as printing directly onto pre-existing structures, handling multiple orientations, and managing complex geometries. Experimental validation was conducted using a robotic Additive Manufacturing setup, demonstrating the fabrication of a fixed glass window frame prototype with varied material properties during printing. The window frame was 3D-printed in 4 hours, 10 minutes, and 34 seconds. Findings suggest that on-substrate Additive Manufacturing with thermoset polymers is a viable approach, offering potential for streamlined construction and enhanced customisation, laying the groundwork for scalable, automated façade construction.

Keywords
On-substrate Additive Manufacturing; Varying Property Additive Manufacturing; Robotic 3D Printing; Thermoset Reactive Polymers; Design-to-Fabrication; Window-Frame; Building Façade

DOI
http://doi.org/10.47982/jfde.2026.351

1 INTRODUCTION

Over the past decade, digital fabrication methods such as Additive Manufacturing (AM) have emerged as a significant research field in the construction and manufacturing of buildings and their components (Hasani & Dorafshan, 2024; Hassan et al., 2024; Leschok et al., 2023; Robayo-Salazar et al., 2023; Wolf, Rosendahl, & Knaack, 2022). The integration of AM in construction processes enables almost seamless digital design-to-fabrication workflows, directly connecting digital design tools with automated fabrication technologies to create components from digital models (Jenny et al., 2023; Hack et al., 2020). This advancement minimises manual intervention and mitigates the traditional disconnect between the design and construction phases, which are often managed by different entities, leading to fragmentation and potential inefficiencies (VHV-Bauschadenbericht, 2022; McKinsey Global Institute, 2017; Kolarevic, 2004). In contrast, integrating AM into digital workflows not only addresses these issues but also unlocks new possibilities for building and component design (Calignano & Mercurio, 2023; Gramazio et al., 2014).

Buildings are traditionally constructed in a sequential order, with individual components and material layers building up on each other. Building façades, in particular, offer significant potential for direct integration with AM workflows. Façade components are typically installed within pre-existing structures and often comprise diverse materials and custom-fit components to meet technical, environmental, and user demands (Herzog, Krippner, & Lang, 2017; Meijs & Knaack, 2009; Knaack et al., 2007). As a result, installing façade components is often manual and labour-intensive, highlighting the need for more efficient solutions.

Traditional manufacturing and installation of window frames, for instance, involve multiple discrete steps, from component fabrication to assembly and on-site installation (Stark et al., 2016; RAL-Gütegemeinschaft Fenster und Haustüren e.V., 2014; British Plastics Federation, n.d.). Each step requires precise measurements, efficient communication between the parties involved, significant manual labour, and depends heavily on the availability of skilled labour, which is increasingly difficult to secure (Juricic, Galic, & Marenjak, 2021).

Despite the potential benefits, integrating AM into façade construction faces challenges, such as size constraints that are not well-suited to the typical dimensions of construction projects and the site-specific nature of building projects (Zuo et al., 2023). Furthermore, most AM processes are restricted to operating within specific spatial boundaries. Consequently, components manufactured through such AM processes still require manual installation, extensive planning, precise scheduling, and secure transportation and logistics (Leschok et al., 2023). Fully leveraging AM in building façades requires both suitable materials and effective integration into sequential build-up processes.

While the implementation of AM in construction is becoming increasingly popular, the overarching topic of robotics and on-site automation has already been investigated and applied for several decades, with approaches for both off-site and on-site construction automation and automated façade installation (Wang et al., 2024; Saidi, Bock, & Georgoulas, 2016). Building upon this, current research into robotic AM introduces novel opportunities for on-site automation. It enables a shift from the assembly of discrete, predefined elements, which is common in traditional construction robotics, towards the continuous material deposition of non-standard, geometrically complex structures (Dielemans et al., 2024; Dörfler et al., 2022; Minibuilders, n.d.).

Currently, 3D concrete printing is the most widely adopted form of AM in construction (Hasani & Dorafshan, 2024; Hassan et al., 2024; Robayo-Salazar et al., 2023). However, it has limited relevance for façades due to their specific and diverse requirements. Research on AM with alternative materials, such as metal (Wynne et al., 2022; Mohsen, 2020; Strauss, 2012), and polymers (Burger et al., 2020; Taseva et al., 2020; Sarakinioti et al., 2018), typically involves separate manufacturing of components that are manually installed, like traditional construction practices.

The use of thermoset reactive polymers in AM offers promising potential to address these challenges. Unlike more established AM processes, thermoset reactive polymers, such as polyurethane, can form adhesive bonds with pre-existing structures, opening the potential for 3D printing directly onto an existing substrate (Defonseka, 2019). This approach also allows for the incorporation of varying material properties throughout the 3D print, representing an advancement over mono-material AM methods (Pajonk et al., 2024). This enables the integration of multiple functions into a single component, enhancing part consolidation and expanding the range of applications for building façades (Strauss, 2012; Nazir et al., 2023b; Pajonk et al., 2022; Grigoriadis, 2015; Wiscombe, 2012).

The use of multi-axis robotic arms in AM is another critical factor for integrating AM into building façades (XtreeE, n.d.; CyBe Construction B.V., 2024; Digital Building Technologies, ETHZ, 2020; MX3D, 2024; Feucht et al., 2022; Cheibas et al., 2022; Tenpierik et al., 2018). The flexibility of robotic arms to orient their end effector at various angles can be leveraged for non-planar AM, allowing components to be 3D-printed in non-horizontal orientations or across curved surfaces (Feucht et al., 2022; Mitropoulou et al., 2024; Bhooshan et al., 2018). Additionally, mobile robotic platforms that combine navigation technology with robotics enable autonomous operation in construction environments, further enhancing the applicability of AM in construction (Jenny et al., 2023; Dielemans et al., 2024).

Building on prior research, this study explores a robotic additive manufacturing (AM) setup using thermoset reactive polymers to fabricate a window frame directly onto an existing substructure–an on-substrate AM approach in which material is deposited layer-wise on the final receiving substrate, defined by the as-built geometry, and combining fabrication and installation in one operation, with potential for future application in building construction.

Previous research (Pajonk et al., 2024) presented a framework for AM with varying material properties of a thermoset reactive polymer. Building upon this, the aim of this research is to implement this method for the on-substrate fabrication of a fixed glass window frame prototype, presenting a novel method with potential for on-site digital fabrication in façade construction.
To achieve this, laboratory experiments were conducted to assess the process's capability to: (i) 3D print across different orientations, including non-horizontal and inverted overhead; (ii) navigate 90° inner corners. To apply this approach, the research proposes a workflow that integrates on-substrate AM digitisation of a window frame installation, which is experimentally validated by directly fabricating a window frame prototype into a pre-existing wooden subframe.

The paper is structured as follows: Section 2 details the methodology and workflow for on-substrate AM of a fixed glass window frame. Section 3 presents the results from the initial process parameter studies to the final workflow demonstration. Section 4 discusses key findings and the potential of on-substrate window frame fabrication. Finally, section 5 summarises the conclusion and future research directions.

2 MATERIALS AND METHODS

2.1 ROBOTIC ADDITIVE MANUFACTURING SETUP

2.1.1 Material System

The thermoset reactive polymer, polyurethane, was used to fabricate a window frame on the substrate. The polyurethane system, provided by Covestro, comprises an isocyanate component, Desmodur N3600, and two polyol components. Both polyol components, Desmophen VP LS 2249/1 and Desmophen VP LS 2328, can be used interchangeably with the isocyanate component, resulting in different mechanical properties of the cured polyurethane. Different colourations of the polyol components were used to distinguish the polyurethane compositions: blue for hard-cured and pink for flexible-cured polyurethane. To enhance the material's rheology for AM, a thickening agent (8,5 wt% CAB-O-SIL TS530) was added to both the isocyanate and polyol components. Table 1 provides an overview of the polyurethane compositions and their individual mechanical properties.

TABLE 1 *Polyurethane materials and their properties used in the AM process.*

Material description	Type	Trade name	Thickening agent	Thickening agent quantity (wt%)	Color	Tensile strength (N/mm^2)	Tear strength (N/mm)	Shore hardness
Hard-cured Polyurethane	Isocyanate	Desmodur N3600	CAB-O-SIL TS530	8.5	Blue	22.6	98.0	Shore 70 D
	Polyol	Desmophen VP LS 2249/1	CAB-O-SIL TS530	8.5				
Flexible-cured Polyurethane	Isocyanate	Desmodur N3600	CAB-O-SIL TS530	8.5	Pink	3.8	5.6	Shore 60 A
	Polyol	Desmophen VP LS 2328	CAB-O-SIL TS530	8.5				

2.1.2 Robotic Additive Manufacturing Platform

As illustrated in Figure 1, the robotic AM setup comprises a modified Viscotec vipro HEAD 5/5 extruder head (Figure 1a) (ViscoTec Pumpen- u. Dosiertechnik GmbH, 2024), combined with a material feeding system for transporting the individual components of the polyurethane system (see Figure 1b, c, and d) to the extruder head. The material feeding system includes several cartridges housed in metal sleeves that transport the components to the extruder head with a constant air pressure of ~40 psi. A static mixing nozzle (Figure 1e) is attached to the outlet of the extruder head, mixing both components of the polyurethane. The extruder head is mounted to the end effector of a 6-axis Universal Robots UR5 collaborative robot arm (Figure 1f), with a reach of 850 mm and a payload of 5 kg (Universal Robots A/S, 2016). A custom controller (Figure 1g) for the extruder head is connected to the main UR5 controller (Figure 1h), managing extrusion start/stop, material retraction, material flow rate, and material composition during the 3D printing.

For testing purposes, a wooden frame (Figure 1i) was used as a substructure for the on-substrate AM. The wooden frame represents a simplified window reveal and is placed at approximately 440 mm from the centre of the robot arm's mounting base (Figure 1j). Metal brackets (Figure 1k) fasten the wooden frame to a table (Figure 1l) and a surrounding alloy frame structure to prevent unwanted vibrations caused by the robot arm movement.

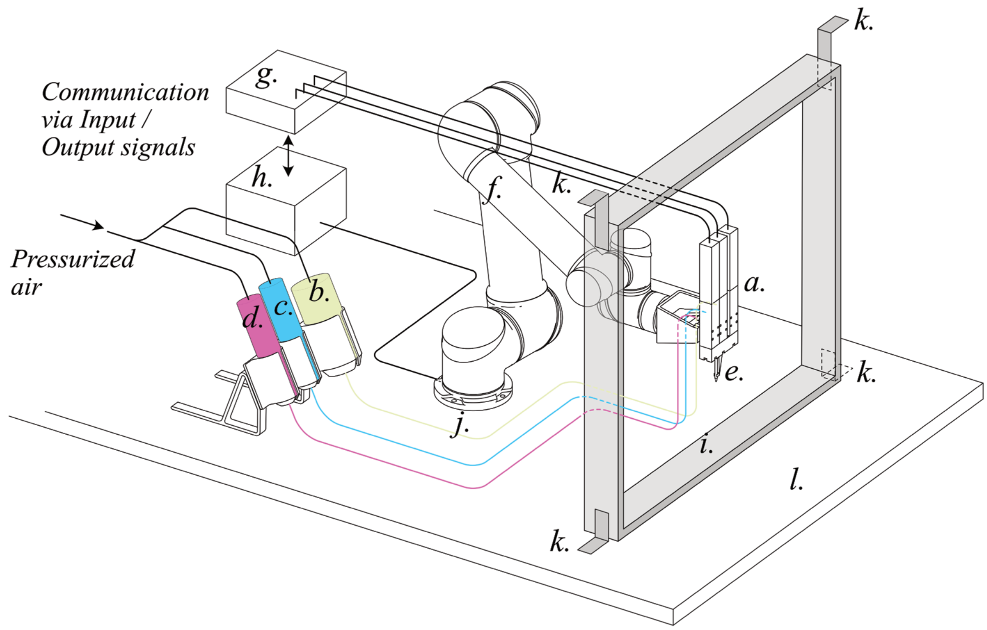

FIG. 1 Schematic illustrating the hardware setup for on-substrate AM: (a) extruder head, (b) Des-modur N3600, (c) Desmophen VP LS 2249/1, (d) Desmophen VP LS 2328, (e) static mixer, (f) Universal Robots UR5 collaborative robot arm, (g) extruder head controller, (h) robot arm controller, (i) wooden frame, (j) mounting base of robot arm, (k) metal brackets, (l) table.

2.2 ON-SUBSTRATE ADDITIVE MANUFACTURING WORKFLOW

The workflow for the on-substrate AM of a window frame (Figure 2) comprises five steps, beginning with digitising the substructure, which also serves to reference its position with the robot arm (Figure 2a). The window frame geometry is then generated using the digitised substructure's geometry and the dimensions and location of the planned insulated glass unit (IGU) (Figure 2b). Following this, the window frame geometry is transformed into a robot trajectory and 3D-printing commands, which are combined into a final program for 3D printing the window frame (Figure 2c). Executing the program, the window frame is 3D-printed into the substructure (Figure 2d). After the 3D print, the IGU is installed (Figure 2e).

The 3D modelling and visual programming environment Rhino-3D and Grasshopper (Robert McNeel & Associates, n.d.), in combination with individual Python components, were used for all programming and geometry modelling tasks.

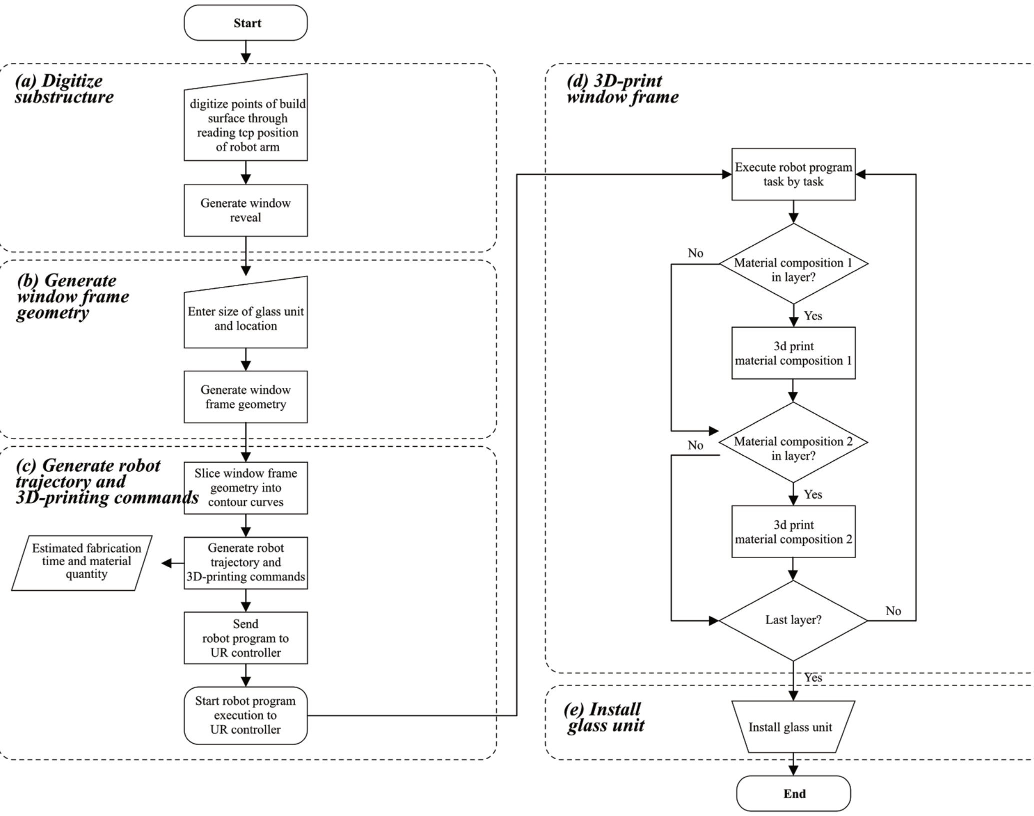

FIG. 2 Flowchart of the workflow for on-substrate AM of a window frame: (a) digitise substructure, (b) generate window frame geometry, (c) robot trajectory and 3D-printing commands, (d) 3D printing window frame, (e) installing glass unit.

2.2.1 Digitising Substructure and window frame geometry

Figure 3 provides an overview of the individual steps required to generate the custom window frame geometry. To generate a digital representation of the inner surface of the window reveal and reference it with the robotic AM setup, the feedback function provided by the Scorpion plug-in (Scorpion, 2024) for Grasshopper was used. This function retrieves the coordinates of the robot arm's tool centre point (TCP) (Figure 3a), relative to the centre of the robot arm's base. The static mixing nozzle tip was set as the TCP, which marks the specific point on the extruder head that defines its position and orientation during material extrusion. Using the extruder head to digitise the reveal's geometry eliminates potential inaccuracies that could otherwise be introduced during a tool change. A custom tip (Figure 3a), with a height of 1.2 mm, was inserted into the static mixer's nozzle to account for the first layer's height, ensuring a consistent offset between the TCP and the window reveal's surface.

The manual movement commands from the robot arm's touch panel were used to navigate the TCP. The corner and centre points were approached and recorded using the Grasshopper script, generating a digital representation of the inner surface with a total of 16 points (Figure 3b).

Following this, the window frame geometry was generated using a second Grasshopper script. Utilising a parametric design approach, this script used the dimensions from the digitised inner surface of the window reveal (Figure 3b) and the dimensions of the IGU (Figure 3c) as input parameters to automatically generate the window frame geometry (Figure 3d). Additional design parameters, including the location and length of the setting and fixation blocks, the positioning of the IGU within the substructure, and the overlap between the window frame and the IGU, were integrated as user-controlled parameters.

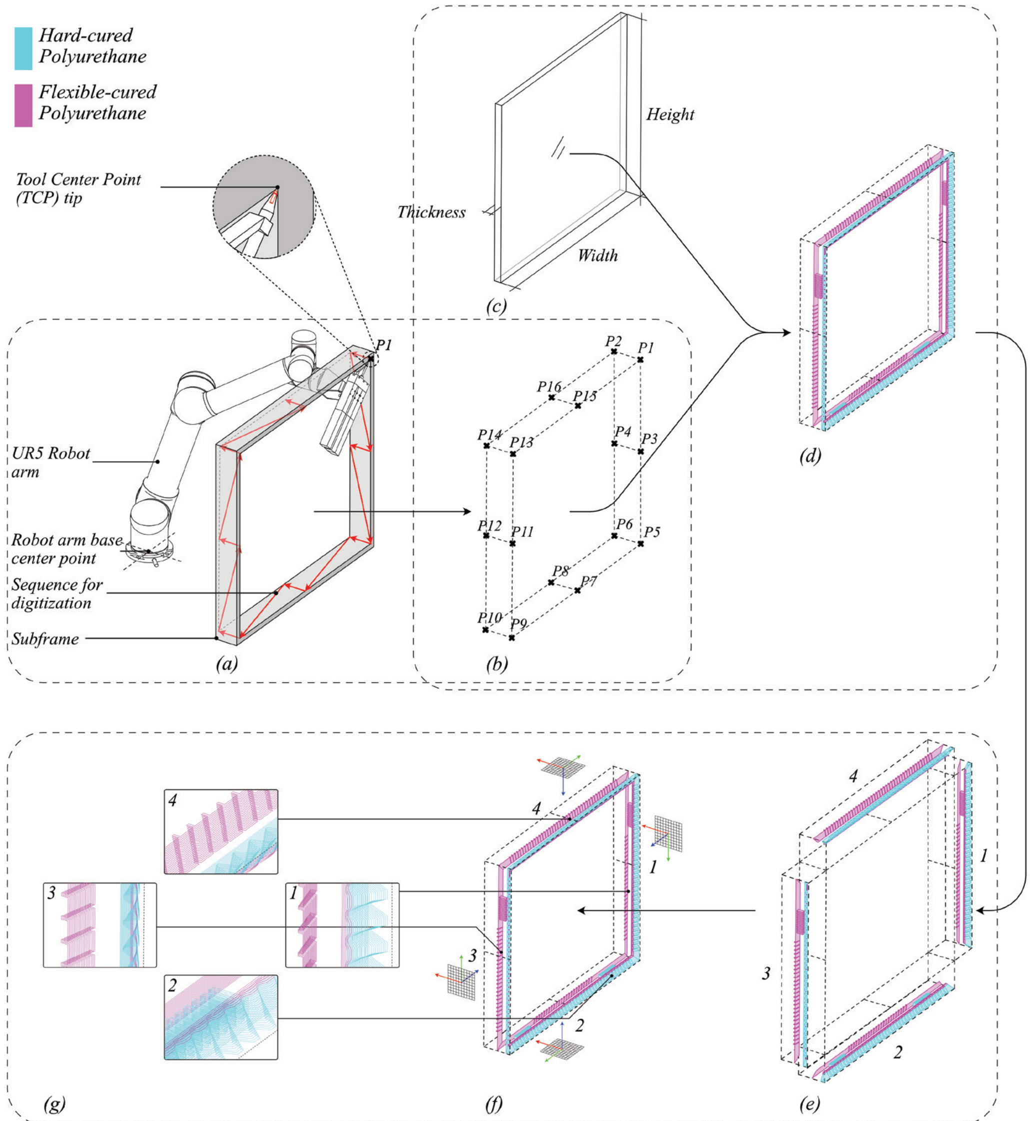

FIG. 3 Diagram illustrating the process from the digitisation of a substructure to the generated design of the window frame: (a) the navigation of the robot arm's TCP within the substructure, (b) the points that are retrieved and form the digital model of the substructure as input data, (c) the dimensions of the insulated glass unit as further input data, (d) the resulting digital model of the prototypical window frame generated by a parametric script, (e) the digital model, which is segmented into four segments, based on the number and orientation of the substructures faces, (f) the resulting individual planes with the Z-Axis oriented perpendicular to each face (g) based on the planes, the sliced segments.

2.2.2 Generate Robot Trajectory and 3D printing commands

The window reveal used in this research consisted of four inner faces. To 3D print the window frame geometry directly into the substructure, the slicing orientation of the geometry had to be adapted to the orientation of each face. As a consequence, the window frame geometry was divided into four segments, each aligning with the window reveals corresponding face orientation (Figure 3e). The segmented geometries were then sliced into layers of polylines, which represent the print path for the robotic AM platform (Figure 3f, g).

The robot trajectory for 3D printing the window frame prototype was generated using the print paths from the sliced segments, travel paths that guide the robot arm between the individual print paths, and additional waypoints that ensure repeatable movement of the robotic AM platform during the layer-wise buildup across the different orientations of the window frame. Additionally, the robot trajectory was designed to also facilitate the use of different material compositions. Therefore, the 3D printing of a single layer follows a specific procedure, described by a cycle executed for each material composition within the layer.

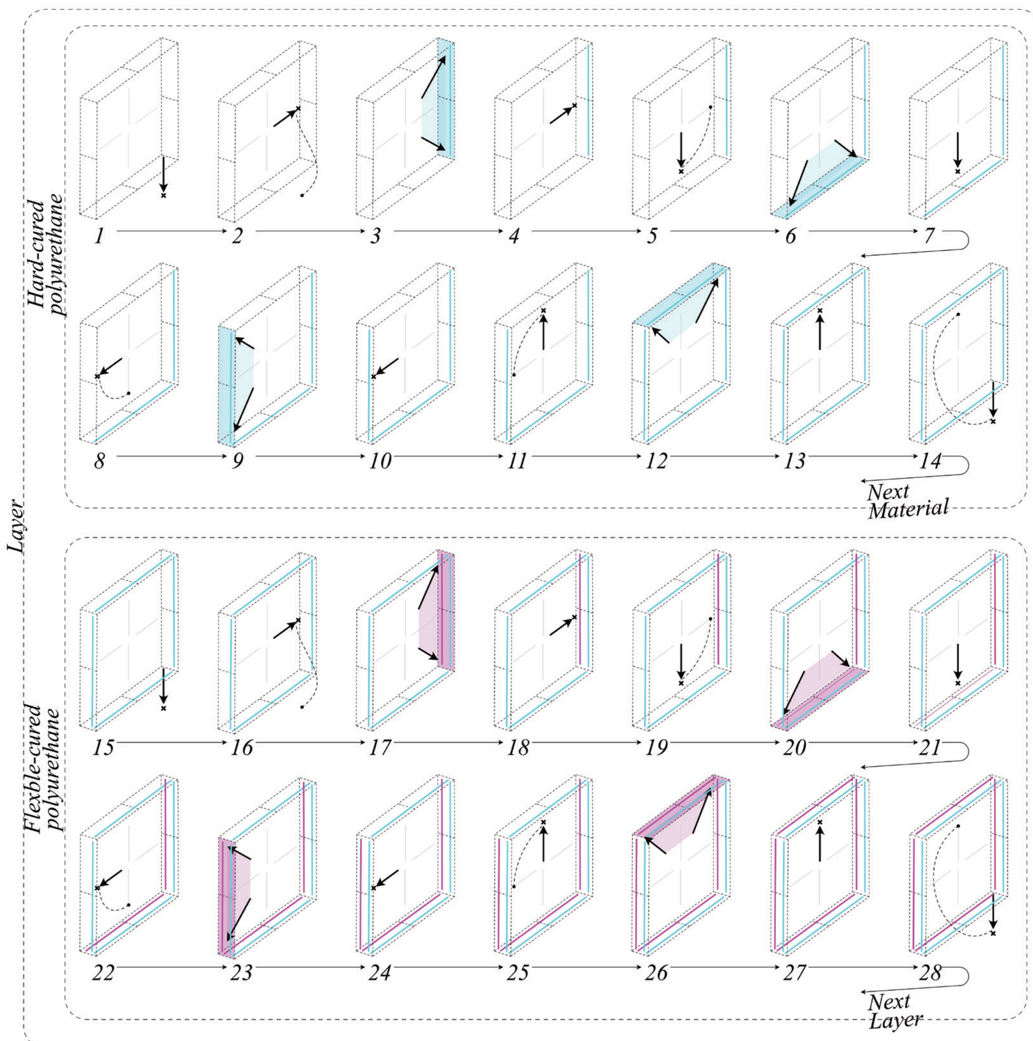

FIG. 4 Diagram illustrates the AM procedure for a single layer of 3D printing across 4 different orientations and with two different polyurethane mixtures.

As illustrated in Figure 4, each layer of the window frame is 3D-printed in a clockwise direction, following steps 1 to 28. Within each layer, a fixed cycle is repeated for each material composition, steps 1 to 14 for the hard-cured polyurethane and steps 15 to 28 for the flexible-cured polyurethane. An optional material discharge at the start of each cycle allows for discharging the former material composition, steps 1 and 15 in Figure 4.

This procedure is repeated for each layer of the window frame geometry. The procedure includes compulsory steps to ensure a consistent robot trajectory and smooth transitions between the different segments of the window frame, steps 1, 2, 5, 8, 11, 14, 15, 16, 19, 22, 25, and 28, and optional steps such as executing a print path, steps 5, 3, 4, 6, 7, 9, 10, 12, 13, 15, 17, 18, 20, 21, 23, 24, 26, and 27 (Figure 4).

The final robot trajectory was compiled into an UR script using the Robots plug-in for Grasshopper [47]. Additional commands for material composition, extrusion start/stop, and pauses were added to the UR script. The robot program was sent to the robot arm's main controller over a local area network via an Ethernet interface.

2.3 DETERMINATION OF CRITICAL PROCESS PARAMETERS

Preliminary experimental investigations were conducted to ensure the successful on-substrate AM of the window frame prototype, particularly addressing the challenges posed by non-horizontal printing orientations. These studies aimed to identify and optimise critical process parameters related to layer adhesion, geometric stability, and the execution of features such as inner corners. The findings from these experiments, detailed below, directly informed the parameter selection and path planning strategies for the glass frame prototype fabrication (Section 3.3).

2.3.1 Methodology for Layer Time and Height Investigation

In AM with thermoset reactive polymers, the curing time after mixing both components is critical, as it determines the time required before an additional layer can be deposited. Consequently, insufficient layer time may result in the deformation or collapse of the 3D-printed geometry. This issue is particularly relevant when a robotic AM platform is employed in conjunction with the AM of thermoset reactive polymers, as this configuration enables 3D printing objects on non-horizontal surfaces and even in an inverted, overhead orientation.

This investigation aimed to quantitatively assess the influence of layer time and layer height on the geometric stability and surface quality of structures printed with the thermoset reactive polyurethane, particularly under non-horizontal conditions where gravitational forces on uncured material can lead to deformation.

The robotic AM setup detailed in Section 2.1 was employed. A specific test geometry, designed to simulate sections of non-horizontal printing and to provide measurable surfaces, was 3D printed into a wooden frame, as depicted in Figure 5a. The material system comprised polyurethane compositions detailed in Table 1. Constant printing parameters for these tests included a print speed of 25 mm/s, a material flow rate of 3 g/min, and a nozzle diameter of 1.19 mm.

Two primary parameters were varied:

- Mean Layer Time: The mean layer time was systematically altered by incorporating additional, distinct geometric elements within the printing path of each layer, while the print speed remained constant. This approach resulted in specimens fabricated with different mean layer times, ranging from approximately 2 minutes 58 seconds to 7 minutes 38 seconds (Specimens A, B, C, D, E in Table 2), as illustrated conceptually in Figure 5b.
- Layer Height: For specimens printed with an extended mean layer time (approximately 7 minutes 38 seconds), the layer height was varied across values of 0.9 mm, 0.925 mm, and 0.95 mm.

Geometric deviation was the main metric for assessment, evaluated based on the mean and standard deviation (SD) of the collected measurements. As illustrated in Figure 5a, deformation was measured along a specific section of each 3D-printed specimen. Measurements were taken at 3 mm intervals to determine the perpendicular distance between a fixed horizontal reference line and the surface of the 3D-printed geometry. The initial measurement point on this line was designated as a zero-deviation reference. Additionally, visual inspection of the printed specimens was performed to assess surface quality and layer evenness.

2.3.2 Methodology for Inner Corner Printing Strategy Evaluation

Navigating inner corners is a significant challenge for on-substrate AM, particularly when printing across differently oriented surfaces. The static mixer nozzle of the extruder head must be positioned at an inclined angle to access the corner without colliding with the substructure, as illustrated in Figure 7. To determine the most effective method for minimising defects in this scenario, an experiment was designed to test different printing strategies.

The experiments utilised the robotic AM setup (Section 2.1) and the polyurethane material system (Table 1). A single-wall test geometry was 3D printed into a wooden frame substructure. This geometry involved forming four inner corners, each approximating a 90° angle, and building up to a total height of 21 mm. Constant process parameters for this study included a layer height of 0.95 mm (based on findings from Section 2.3.1), a print speed of 25 mm/s, and a material flow rate of 3 g/min.

Three distinct nozzle path strategies for navigating these inner corners were evaluated, as illustrated in Figure 8:

- Strategy (a): Moving the nozzle in a continuous motion from one corner of the frame to the opposite corner.
- Strategy (b): Printing from the middle of one side to the corner and continuing in a continuous motion to the middle of the adjacent side.
- Strategy (c): Extruding from a corner towards the middle, then executing a travel move (non-extruding) to the next corner, and resuming extrusion back towards the middle.

A semi-quantitative assessment was conducted to provide a structured comparison of the complex surface qualities. The quality of each corner strategy was scored against a rubric of defined criteria, each on a five-point scale (1=Poor, 5=Excellent). The criteria were: (i) Geometric Fidelity, assessing how closely the print resembled a sharp 90° corner; (ii) Surface Evenness, evaluating the texture for smoothness versus wrinkles or smearing; and (iii) Path Integrity, inspecting for tears or gaps within the printed bead. As print quality was observed to be lower in the upper corners, the scores for each strategy were assigned based on the worst-observed defects to represent a conservative performance analysis. In addition to the scored criteria, nozzle contamination was observed for each strategy, as material buildup on the static mixer directly impacts continuous operation and overall print quality.

3 RESULTS

3.1 INFLUENCE OF LAYER TIME AND HEIGHT ON GEOMETRIC STABILITY IN NON-HORIZONTAL PRINTING

The investigation into the effect of layer time on the geometric stability of non-horizontal prints revealed a direct correlation between longer layer times and reduced gravitational deformation. The results of this study are presented in Table 2 and visualised in Figure 6.

Increasing the mean layer time from 2:58 (Specimen A) to 7:37 (Specimen C) led to a 73.4% reduction in the mean geometric deviation, from 0.88 mm to 0.234 mm. The Standard Deviation (SD) provided further insight into print consistency. Specimen A exhibited a high SD of 0.33mm, reflecting a high deviation between the individual measurement points. While increasing the layer time (Specimen C) reduced the mean deviation, the relatively high SD of 0.22 mm underlines the observed "minor surface irregularities". The subsequent adjustment of the layer height to 0.95 mm (Specimen E) proved to be an effective countermeasure, minimising not only the mean deviation to 0.056 mm but also the SD to just 0.03 mm, which indicates a print that is both accurate and consistent.

Based on these findings, the parameters for Specimen E (layer height of 0.95 mm and a minimum layer time of ~7.6 minutes) were identified as optimal. This combination maximised both geometric accuracy (lowest mean deviation) and consistency (lowest standard deviation) of the print, ensuring high geometric quality for the main demonstrator.

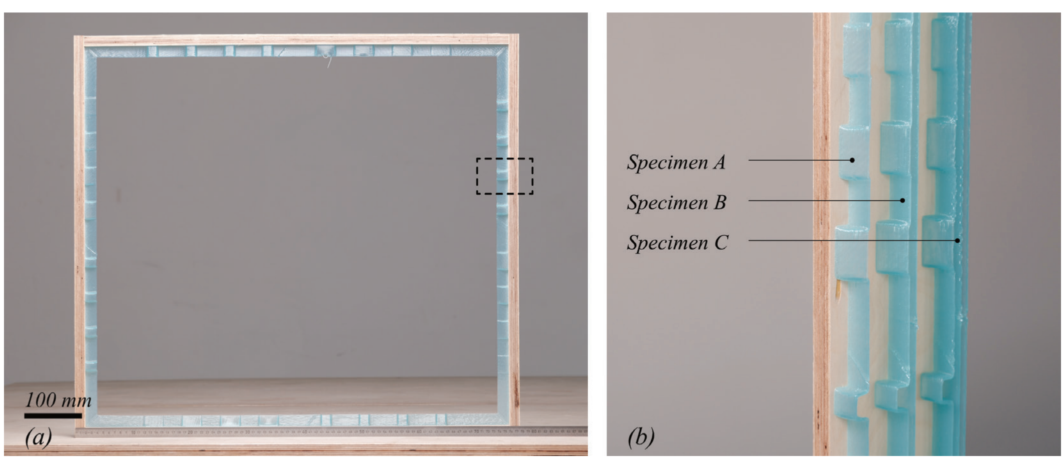

FIG. 5 (a) Image shows the test geometry fitted into a wooden frame and the section of the geometry used for the deviation measurements, (b) image shows specimen A, B, and C of on-substrate AM with one additional element for specimen B, and two additional elements for specimen C.

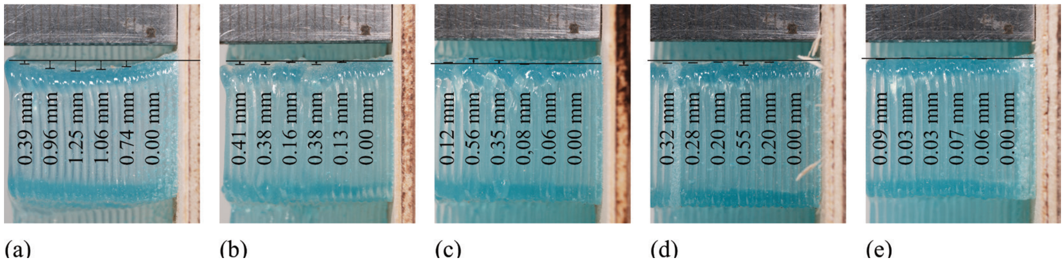

FIG. 6 Image shows the sections of the 3D-printed specimens where the distance between the 3D-printed geometry and an ideal perpendicular oriented line was measured: (a) specimen A with layer time 2 minutes 58 seconds and layer height 0.9 mm, (b) specimen B with layer time 5 minutes 17 seconds and layer height 0.9 mm, (c) specimen C with layer time 7 minutes 37 seconds and layer height 0.9 mm, (d) specimen D with layer time 7 minutes 38 seconds and layer height 0.925 mm, (e) specimen E with layer time 7 minutes 38 seconds and layer height 0.95 mm.

TABLE 2 *3D printing parameters and metrics, including measurements and deviations between the 3D-printed geometry and an ideal perpendicular line within a single specimen.*

Specimen	Layer height [mm]	Mean Layer time [h:m:s]	Measure 1 [mm]	Measure 2 [mm]	Measure 3 [mm]	Measure 4 [mm]	Measure 5 [mm]	Mean deviation [mm]	Std. Deviation [mm]
A	0.9	0:02:58	0.74	1.06	1.25	0.96	0.39	0.88	0.33
B	0.9	0:05:17	0.13	0.38	0.16	0.38	0.41	0.292	0.14
C	0.9	0:07:37	0.06	0.08	0.35	0.56	0.12	0.234	0.22
D	0.925	0:07:38	0.2	0.55	0.2	0.28	0.32	0.31	0.14
E	0.95	0:07:38	0.06	0.07	0.03	0.03	0.09	0.056	0.03

3.2 EVALUATION OF INNER CORNER PRINTING STRATEGIES

The three corner printing strategies were evaluated to identify the optimal method for navigating 90° corners while minimising print defects.

TABLE 3 *Assessment and qualitative observations of the three corner printing strategies.*

Strategy	Geometric Fidelity	Score (1-5)	Surface Evenness	Score (1-5)	Path Integrity	Score (1-5)	Total Score (/15)
(a)	Poor fidelity, all corners rounded and distorted.	2	Very poor, strong smearing and wrinkles on all corners.	2	Poor, large open tears in one corner, small holes in others.	2	6
(b)	Good, path was fully closed and completed on all corners.	4	Very poor, strong smearing and wrinkles on upper corners.	2	Far, a few small holes visible in its path.	3	9
(c)	Fair, 3 of 4 corners were sharp. Path failed to close in one corner.	3	Good, only minor smearing and unevenness visible.	4	Fair, a single propagating tear in the upper right corner.	3	10

The semi-quantitative evaluation revealed distinct performance tradeoffs, as summarised in Table 3. While no single strategy proved perfect, Strategy (c) achieved the highest total score, demonstrating the best overall balance of properties. Its key advantage was superior Surface Evenness (4/5) compared to strategies (a) and (b), which involved extruding while approaching the corner. This resulted in lower scores on Surface Evenness and Path Integrity, due to smearing and wrinkles, particularly in the upper layers of the print (Figure 9a, b). In addition, nozzle contamination required frequent cleaning throughout the 3D print. In contrast, Strategy (c) avoided these contamination issues.

Although Strategy (c) had only fair Geometric Fidelity (3/5) due to a minor tear on one corner, its process stability and avoidance of nozzle buildup made it the most reliable option for a long-duration print. Its primary tradeoff, the introduction of additional seams at the start and end of each printed segment, was deemed an acceptable compromise for achieving a reliable 3D print. Therefore, Strategy (c) was selected as the optimal approach for the final window frame demonstrator.

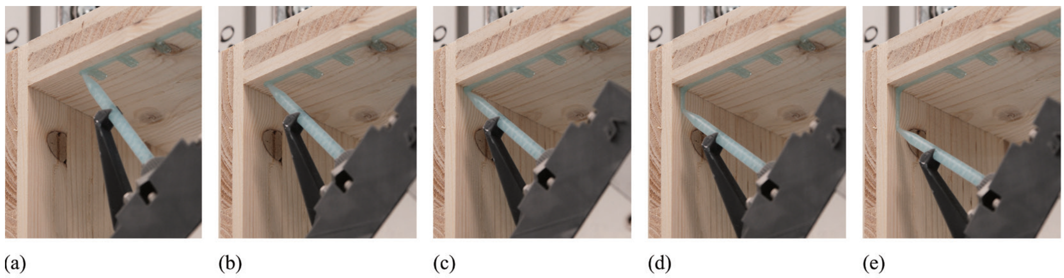

FIG. 7 Images showing the 3D printing of an inner corner, (a and b) approaching a corner while extruding, (c) turning point of the corner, (d and e) departing a corner while extruding.

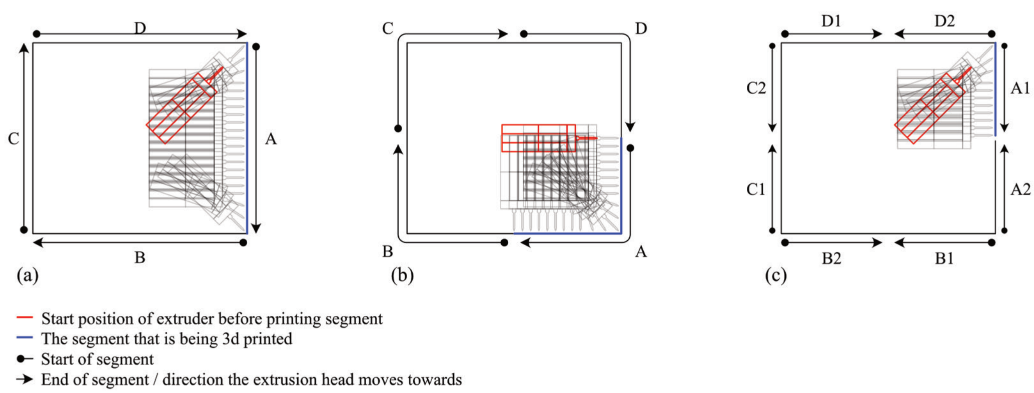

FIG. 8 Diagrams illustrating different strategies for 3D printing inner corners, (a) moving the nozzle from one corner of the frame in a continuous motion to the opposite corner, (b) starting from the middle of one side, moving to the corner, and continuing in a continuous motion to the middle of the next side, (c) starting at the first corner, moving to the middle while extruding, traveling to the second corner, and finally returning to the middle using a two-step motion.

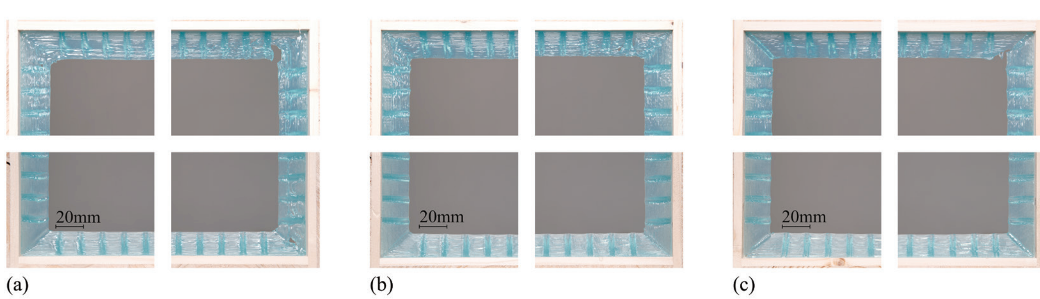

FIG. 9 Images showing the resulting corners of the different strategies, (a) moving the nozzle from one corner of the frame in a continuous motion to the opposite corner, (b) starting from the middle of one side, moving to the corner, and continuing in a continuous motion to the middle of the next side, (c) starting at the first corner, moving to the middle while extruding, traveling to the second corner, and finally returning to the middle using a two-step motion.

3.3 DEMONSTRATION OF THE 3D-PRINTED WINDOW FRAME PROTOTYPE

Applying the optimal parameters identified in the preliminary investigations, the complete design-to-fabrication workflow was demonstrated by fabricating a prototypical fixed glass window frame. This final experiment served to validate the proposed workflow and test the feasibility of using thermoset reactive polymers for on-substrate AM.

The workflow was initiated with the generation of a digital representation of the wooden frame by recording the frame's corner and centre points (Figure 10a). The resulting surface model represented the as-built situation and served as the window reveal for subsequent on-substrate AM. The recorded corner and centre points resulted in a window opening of approximately 741 mm x 663 mm with a depth of 99 mm. The insulated glass unit measured 720 mm x 640 mm with a thickness of 24 mm (Figure 10b).

Subsequently, a model of a window frame geometry was generated using the parametric algorithm within the Grasshopper environment, which incorporated the dimensions of the subframe model and the insulated glass unit as input data. Figure 10c illustrates the window frame's design concept, which comprises three distinct sections: the outer section, the middle section, and the inner section. Each section fulfils a specific function and has been adapted to the input data accordingly. The glass unit was positioned in the centre of the subframe. The different material properties were assigned to the window frame geometry as part of the model-generating algorithm.

The complete model was divided into four segments, each representing one side of the window frame. The segments were then sliced into layers of polylines with a layer height of 0.95mm, representing the intended 3D print path. A total of 599 individual print paths were generated across 24 layers, comprising 154.70 m of print path length for the hard-cured polyurethane, 114.13 m for the flexible-cured polyurethane, and 376.34 m of travel path between the individual print paths. The slicing orientation for the segments was defined in accordance with the orientation of each segment's substructure, as described in Section 2.2.2. The corners of the window frame were 3D-printed using Strategy (c), resulting in seams at both the corners and the centre of each side. The total height of the window frame ranged from 19.46 mm to 22.45 mm. Both hard-cured and flexible-cured polyurethanes were integrated into the window frame design and executed accordingly, following the 3D printing procedure described in Section 2.2.3.

Figure 11 shows the fabrication process of the window frame prototype. The window frame was fabricated in a single 3D print session, totalling 4 hours, 10 minutes, and 34 seconds. The mean layer time was 10 minutes and 24 seconds, with the shortest being 2 minutes and 55 seconds for the final layer and the longest being 19 minutes and 57 seconds for the first layer. The process parameters used to fabricate the window frame are documented in Table 4. A comprehensive breakdown of the 3D print metrics, including the individual tasks and their respective time consumption, is documented in Table 5.

Following fabrication, the window frame prototype was left to rest for at least 24 hours before the glass unit was installed. Figure 12 illustrates the window frame prototype with the glass unit installed.

TABLE 4 *Process variables used for the fabrication of the window frame prototype.*

Process variable	Value	Unit
Print Speed	25	mm/s
Travel Speed	150	mm/s
Acceleration	300	mm/s^2
Nozzle Diameter	1.19	mm
Layer height	0.95	mm
Material flow rate	3	g/min
Material discharge time	22	s
Pause before and after extrusion	0.5	s

TABLE 5 *Resulting 3D print metrics from the fabrication of the window frame prototype.*

3D print metric	Value	Units
Robot arm trajectory: Extrusion	268.84	m
Robot arm trajectory: Travel	376.34	m
Layer count	24	
Material discharge	37	
Individual 3d print lines	599	
Time: Extrusion	3:04:12	h:m:s
Time: Travel	0:51:24	h:m:s
Time: Material discharge	0:14:57	h:m:s
Total time for 3d printing	4:10:34	h:m:s

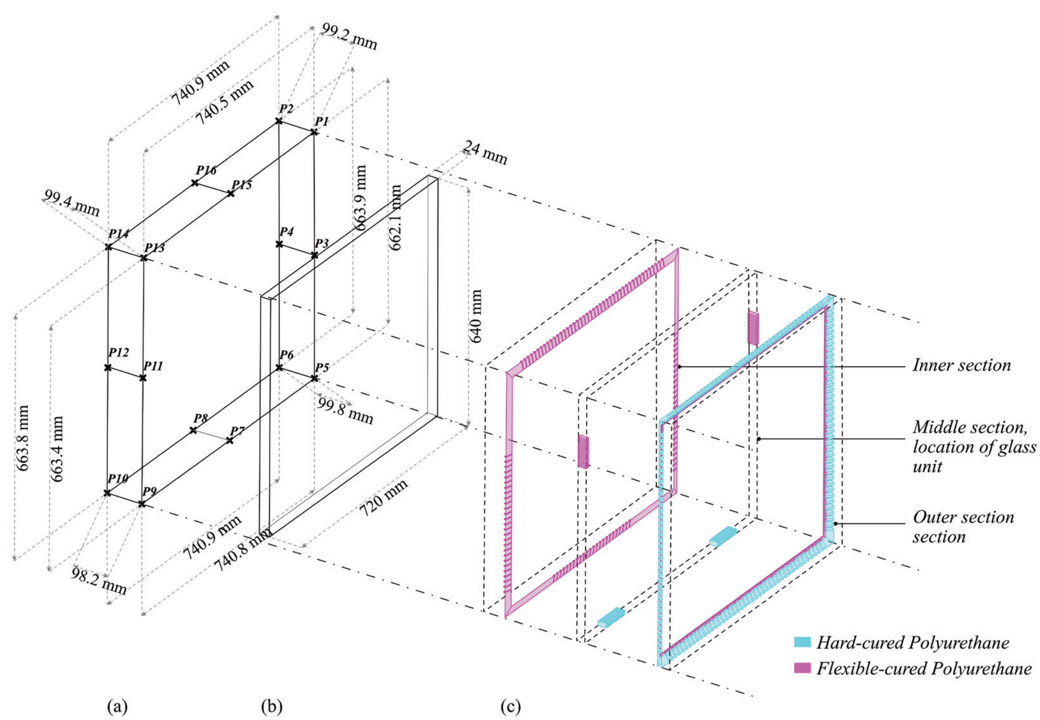

FIG. 10 Diagram illustrating (a) the digitised points that represent the reveal for the window frame (the wooden subframe), (b) the insulated glass unit to be installed into the opening, and (c) exploded-view drawing of the generated window frame geometry, based on both inputs and consisting of an inner, middle, and outer section.

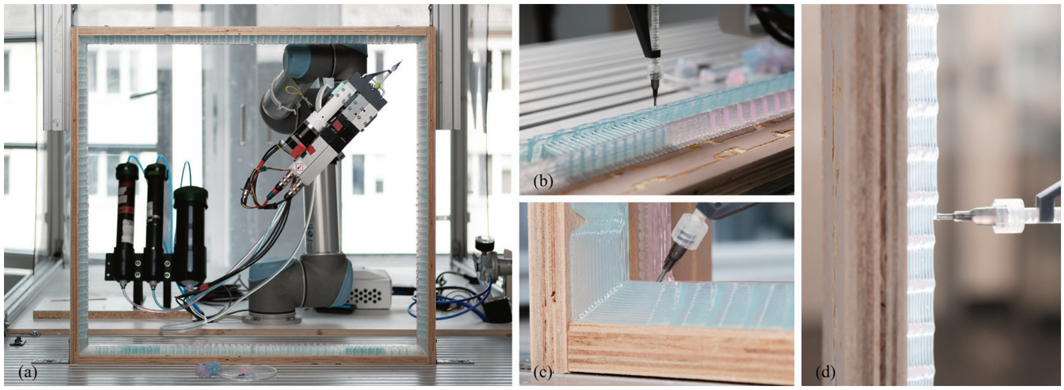

FIG. 11 Image showing (a) the fabrication of the window frame prototype, mounted in a laboratory setup, (b) 3D printing different material properties next to each other, (c) executing an inner corner of the window frame at an inclined angle, (d) 3D printing in a non-horizontal manner.

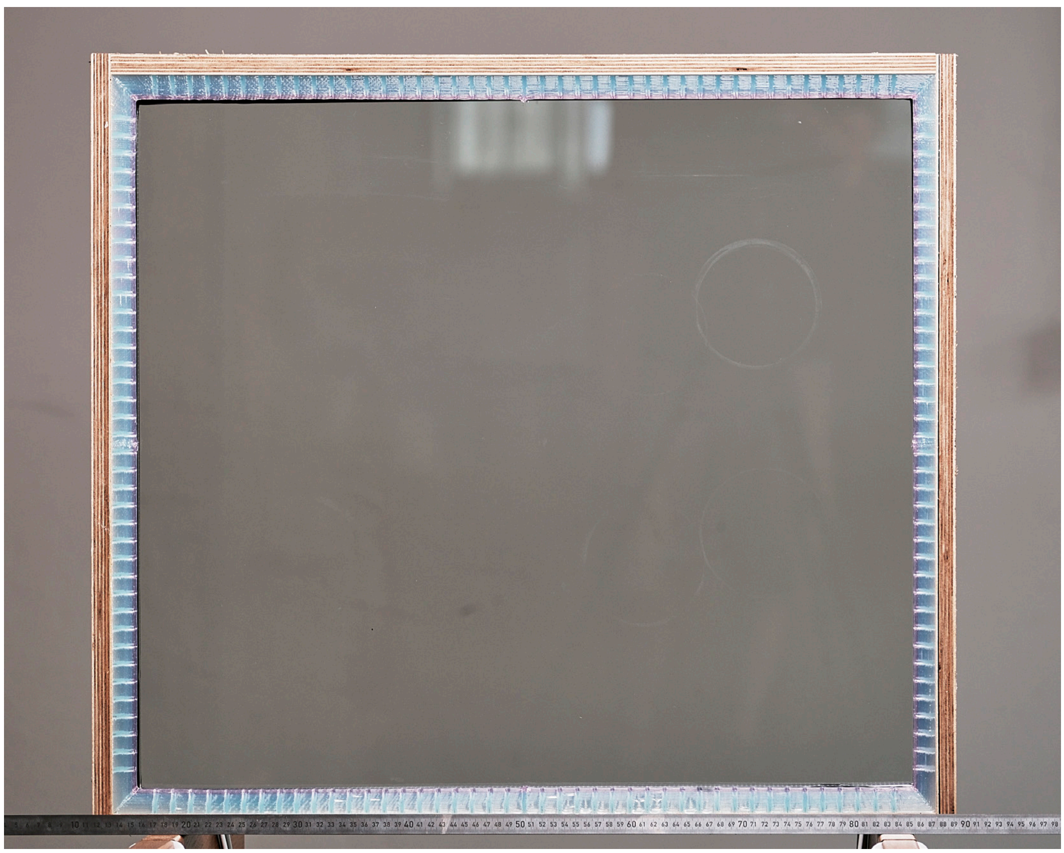
FIG. 12 Image illustrates the 3D-printed window frame with the IGU installed.

4 DISCUSSION

The use of AM with thermoset reactive polymers presents distinctive advantages, including the ability to operate independently of an energy-intensive heat source (Rios et al., 2018), the ability to produce large-scale objects (Romberg et al., 2022), high volumetric flow rates, and isotropic material properties in the transverse orientation (Uitz et al., 2021). Additionally, AM with thermoset reactive polymers allows for varying material properties during 3D printing (Pajonk et al., 2024; Uitz et al., 2023) and has the potential to create an adhesive bond between the thermoset reactive polymer and pre-existing structures (Defonseka, 2019). These advantages, particularly when used with a six-axis robot arm, support the feasibility of on-substrate AM and its potential application in façade construction scenarios.

The fabrication of the window frame was preceded by understanding the process limitations, particularly the effect of gravity on the uncured polymer during non-horizontal 3D printing. The investigation into layer time (Section 3.1) demonstrated that a minimum time of approximately 7.6 minutes between layers was critical to ensure geometric stability. Shorter times resulted in significant deformation (mean deviation of 0.88 mm), while the optimised parameters reduced this deviation to just 0.056 mm (SD = 0.03mm). This finding highlights a fundamental principle for on-substrate AM with reactive polymers: the overall print size and toolpath length must be sufficiently large to allow for adequate curing time between vertically adjacent depositions, a key consideration for designing future applications. Alternative approaches to mitigate deformation, which were not investigated in this study, include reducing the 3D printing speed or increasing the reaction kinetics of the polyurethane. These approaches may be particularly relevant for smaller geometries that do not meet the minimum layer time requirements.

Navigating geometries like inner corners was identified as another significant challenge. The semi-quantitative evaluation (Section 3.2) revealed that toolpath strategies involving extrusion during corner entry (Strategies a and b) were detrimental to 3D print quality, leading to nozzle contamination and surface defects. The selection of Strategy (c), which avoids this type of extrusion, proved essential for process stability, despite the tradeoff of introducing additional seams. This implies that for reliable on-substrate AM, toolpath generation algorithms must avoid angled extrusion, which causes a "ploughing" effect, favouring segmented paths even at the expense of part continuity.

The practical feasibility of this approach was demonstrated through the use case of a fixed glass window frame measuring approximately 741 mm by 663 mm. The fabrication of the window frame was integrated into a digital design-to-fabrication workflow, beginning with the digitisation of a window reveal, achieved by navigating the TCP of the robotic arm to its corner and middle points. While this approach proved sufficient for the window reveal used in this research, more advanced digitisation techniques could further improve the accuracy of the geometry representation, making it applicable to more complex forms.

Using a parametric algorithm to generate the window frame geometry allowed dynamic adjustments based on the recorded dimensions of the window reveal and IGU, potentially rendering manual drawings or modelling redundant. As a result, the window frame geometry could be precisely aligned with the recorded dimensions, representing the as-built conditions. Consequently, eliminating gaps and joints that are typically required to accommodate tolerances. However, it is crucial to acknowledge that joints are also integral for functional purposes, such as providing watertight and airtight seals and accounting for deformations due to load or materials expansion and shrinkage

(Meijs & Knaack, 2009). Future research should explore how these functional requirements can be integrated into 3D-printed components.

Although the design served as an initial prototype, further refinements and details could be incorporated into the algorithm. The prototype also demonstrated the necessity for a design approach that considers the specific limitations and characteristics of the AM process, such as wall inclination limits and the ability to execute fine details. This prototype was primarily aimed at demonstrating feasibility rather than evaluating the window frame's functional characteristics, such as mechanical strength or thermal performance. Future research should focus on these aspects to comprehensively validate the performance of such components in real-world applications.

The window frame prototype was 3D printed in 4 h, 10 min, and 34 s. This timeframe, while not optimised, provides a baseline for future development of the AM method. The highest potential for enhancing unit throughput lies in print speed, which accounted for approximately 74% of the total time. The material flow rate was set to 3 g/min, corresponding to 2.68 ml/min based on the material volume. The theoretical volumetric flow rate of the extruder head is set to 12 ml/min (ViscoTec Pumpen- u. Dosiertechnik GmbH, 2024), indicating that the extrusion speed could be increased by a factor of 3.48, yielding a best-case scenario per unit of 1 h, 59 min, 17 s.

A fair comparison with conventional window frame manufacturing must consider the entire process chain, not only unit deposition rates. While the unit throughput of continuous profile production (e.g., extrusion/pultrusion) is substantially higher than any current layer-wise AM method, on-substrate AM merges fabrication and installation into a single, integrated operation. For an on-site deployment, the principal steps are: (i) transporting and setting up the system, (ii) preparing the substrate, (iii) digitising the as-built opening, (iv) 3D printing, (v) local rework/finishing, and (vi) connecting interfaces and installing subsequent components (e.g., glazing). By contrast, the conventional prefabrication route entails: (i) profile extrusion, (ii) shop assembly and finishing, (iii) storage and logistics, (iv) transport/hoisting, (v) substrate preparation, (vi) site installation, and (vii) site rework/adjustment. A direct comparison should therefore include the unit cycle time at the window reveal and the order-to-installed lead time. Quantifying each term is beyond the scope of this study, but the outlined framework clarifies that on-substrate AM primarily targets lead-time compression by removing logistics, hoisting, and cross-industry queues, and variability by digitising the as-built opening and automating the installation process. In contrast, factory prefabrication remains advantageous where repetition enables parallelisation and standard detailing is coupled with established construction processes.

The scalability of the on-substrate AM approach to other façade elements presents a significant opportunity for façade construction. Its adaptability to various geometries makes it suitable for a wide range of custom components, including façade panels, decorative elements, and interfaces between different building components. For instance, this approach could also be extended to glass façades, creating customised interfaces between structural elements and glass panels. By leveraging the flexibility of the robotic arm setup and the ability to dynamically vary material properties, this method could cater particularly to non-standard building designs that require tailored solutions and complex geometries. Furthermore, while in this research only sharp transitions between the two polyurethane compositions were realised, future research should focus on functionally graded transitions. This offers various potential for façade design, including reduced stress and strain between the individual material compositions, resulting in reduced material fatigue.

Implementing on-substrate AM in construction combines manufacturing and installation into a single on-site operation. This can streamline logistics, minimise transportation, reduce material waste, and ease dependence on scarce skilled labour. However, these benefits must be weighed against the logistical and operational demands of on-site execution. A particular challenge for on-site implementation is accurate localisation. In the presented workflow, the as-built window opening serves as the substrate that is digitised relative to the robot's coordinate system (Section 2.2.1). While current commercial solutions, such as the Hilti Jaibot, have successfully implemented on-site mobility for tasks like drilling, these operations are generally limited in their movements required for drilling. In contrast, on-substrate AM requires continuous, high-precision 6-axis control to ensure consistent material deposition and layer height, which is significantly more sensitive to environmental disturbances. While the ultimate goal is deployment on a mobile platform, fully autonomous construction in unstructured environments using mobile robots remains a significant hurdle (Dörfler et al. 2024; Melenbrink, Werfel & Menges, 2020). Consequently, this research intentionally utilises a fixed-based setup to decouple the AM process from potential failure risks associated with the complexities of mobile navigation and environmental influences (Kim et al., 2026), focusing on validating the fundamental feasibility of the vertical deposition process.

Looking towards future implementation from a fixed-base to a mobile application, this research could utilise the Mobile Additive Manufacturing framework developed by Dörfler et al. (2022) and demonstrated in the field of robotic repair by Dielemans et al. (2024). In their approach, the robot scans the existing substrate to generate toolpaths that adapt to geometric irregularities. By integrating a similar approach into the window frame fabrication process, the system could compensate for tolerances of the window reveal, effectively treating the window installation as a localised "in-place" manufacturing process.

Furthermore, this research was conducted in a controlled laboratory environment. For on-substrate AM to achieve broader adoption in façade construction, it must be validated across varying climatic conditions, substrate types, and larger architectural elements. Ambient temperature and humidity affect cure kinetics, potentially impacting surface quality and strength. Likewise, the receiving substrate (e.g., concrete) introduces variability, including porosity, moisture, gravel pockets, dust, or release agents, that can impair the bond. Potential mitigations include local environmental control through temporary tenting and substrate preconditioning and preparation through mechanical cleaning, moisture checks, and quick on-site adhesion tests. A priority for future work is to map a process window and define acceptance criteria for bond and finish to enable clear go/no-go decisions.

Another critical future focus should be on the sustainability aspects of the employed materials and proposed methodology. Although on-substrate AM offers advantages over traditional methods, the environmental impact of the materials used and their end-of-life handling needs further investigation. Potential future directions for polyurethane use were discussed by Pajonk et al. (2024), including the use of bio-based polyurethane or recycling approaches. However, a more immediate solution could be to minimise material consumption through optimisation, ensuring material use is kept as low as necessary.

While the method was originally envisioned for on-site construction, its potential for off-site prefabrication should not be overlooked, as it could be equally or more effective.

5 CONCLUSIONS

This research demonstrates the feasibility of using AM with varying properties of a thermoset reactive polymer for on-substrate fabrication of custom-fitted window frames. By developing and validating a comprehensive workflow that integrates digital design with robotic on-substrate AM, this study addresses key challenges in on-substrate AM, such as printing across various orientations, handling complex geometries such as inner corners, and operating directly on pre-existing structures. The successful application of this approach to fabricate a fixed glass window frame highlights the potential to streamline construction processes, reduce manual installation, and enhance customisation. Furthermore, the results show that integrating design-to-fabrication workflows and on-substrate AM has the potential to combine design with manufacturing and installation into a continuous process that allows for better connection of the individual steps, but also higher flexibility.

However, the study was conducted under controlled laboratory conditions, and further research is required to validate these findings in real-world environments. Future work should focus on performance testing of the fabricated components, including mechanical and thermal characteristics, to ensure they meet the demands of building façades. Additionally, scalability assessments are needed to explore how this approach can be adapted to different climatic conditions, various substructures, and larger architectural elements.

Sustainability aspects of the employed materials and processes should be a critical focus moving forward. While on-substrate AM provides clear advantages over traditional methods, the environmental impact of the materials used, including their end-of-life handling, must be thoroughly assessed.

Despite these limitations, this work highlights a novel approach to façade construction that leverages the unique benefits of AM with the thermoset reactive polymer polyurethane, including mass customisation, geometric freedom, and the direct link between design and manufacturing. As such, this research lays the groundwork for further exploration and development, paving the way for more efficient, adaptable, and sustainable construction practices.

Acknowledgments

The authors would like to express their sincerest gratitude to Covestro AG for their support of this research project.

References

Bhooshan, S., Ladinig, J., Van Mele, T., & Block, P. (2018). Function representation for robotic 3D printed concrete. In Springer eBooks (pp. 98–109). https://doi.org/10.1007/978-3-319-92294-2_8

British Plastics Federation. (n.d.). How PVC-U windows and doorsets are made. British Plastics Federation. https://www.bpf.co.uk/windows/how_pvcu_windows__are_made.aspx

Burger, J., Lloret-Fritschi, E., Scotto, F., Demoulin, T., Gebhard, L., Mata-Falcón, J., Gramazio, F., Kohler, M., & Flatt, R. J. (2020). Eggshell: Ultra-Thin Three-Dimensional printed formwork for concrete structures. 3D Printing and Additive Manufacturing, 7(2), 48–59. https://doi.org/10.1089/3dp.2019.0197

Calignano, F., & Mercurio, V. (2023). An overview of the impact of additive manufacturing on supply chain, reshoring, and sustainability. Cleaner Logistics and Supply Chain, 7, 100103. https://doi.org/10.1016/j.clscn.2023.100103

Cheibas, I., Gamote, R. P., Önalan, B., Lloret-Fritschi, E., Gramazio, F., & Kohler, M. (2022). Additive manufactured (3D-Printed) connections for thermoplastic façades. In Lecture Notes in Civil Engineering (pp. 145–166). https://doi.org/10.1007/978-3-031-20241-4_11

CyBe Construction B.V. (2024, June 20). We redefine construction | CyBe Construction. CyBe Construction. https://cybe.eu/

Defonseka, C. (2019). Two-Component polyurethane systems. In De Gruyter eBooks. https://doi.org/10.1515/9783110643169

Dielemans, G., Lachmayer, L., Khader, N., Hack, N., Raatz, A., & Dörfler, K. (2024). Robotic repair: In-Place 3D printing for repair of building components using a mobile robot. In Springer Tracts in Additive Manufacturing (pp. 156–164). https://doi.org/10.1007/978-3-031-64269-2_20

Digital Building Technologies, ETHZ. (2020, March 2). Concrete Choreography - dbt. Dbt. https://dbt.arch.ethz.ch/project/concrete-choreography/

Dörfler, K., Dielemans, G., Lachmayer, L., Recker, T., Raatz, A., Lowke, D., & Gerke, M. (2022). Additive Manufacturing using mobile robots: Opportunities and challenges for building construction. Cement and Concrete Research, 158, 106772. https://doi.org/10.1016/j.cemconres.2022.106772

Dörfler, K., Dielemans, G., Leutenegger, S., Jenny, S. E., Pankert, J., Sustarevas, J., Lachmayer, L., Raatz, A., & Lowke, D. (2024). Advancing construction in existing contexts: Prospects and barriers of 3d printing with mobile robots for building maintenance and repair. Cement and Concrete Research, 186, 107656. https://doi.org/10.1016/j.cemconres.2024.107656

Feucht, T., Waldschmitt, B., Lange, J., & Erven, M. (2022). Additive manufacturing of a bridge in situ. Steel Construction, 15(2), 100–110. https://doi.org/10.1002/stco.202100045

Gramazio, F., Kohler, M., Willmann, J., & Jaeger, R. (2014). The robotic touch: How robots change architecture: Gramazio & Kohler, research ETH Zurich 2005–2013. Park Books. https://ci.nii.ac.jp/ncid/BB15951754

Grigoriadis, K. (2015). Material Fusion: A Research into the Simulated Blending of Materials Using Particle Systems. International Journal of Architectural Computing, 13(3–4), 335–352. https://doi.org/10.1260/1478-0771.13.3-4.335

Hack, N., Dörfler, K., Walzer, A. N., Wangler, T., Mata-Falcón, J., Kumar, N., Buchli, J., Kaufmann, W., Flatt, R. J., Gramazio, F., & Kohler, M. (2020). Structural stay-in-place formwork for robotic in situ fabrication of non-standard concrete structures: A real scale architectural demonstrator. Automation in Construction, 115, 103197. https://doi.org/10.1016/j.autcon.2020.103197

Hasani, A., & Dorafshan, S. (2024). Transforming construction? Evaluation of the state of structural 3D concrete printing in research and practice. Construction & Building Materials, 438, 137027. https://doi.org/10.1016/j.conbuildmat.2024.137027

Hassan, H., Rodriguez-Ubinas, E., Tamimi, A. A., Trepci, E., Mansouri, A., & Almehairbi, K. (2024). Towards innovative and sustainable buildings: A comprehensive review of 3D printing in construction. Automation in Construction, 163, 105417. https://doi.org/10.1016/j.autcon.2024.105417

Herzog, T., Krippner, R., & Lang, W. (2017). Façade Construction Manual. DETAIL. https://doi.org/10.11129/9783955533700

Hilti Jaibot. (n.d.). BIM & Robotik: Das kann der Hilti Bohrroboter. https://www.hilti.de/content/hilti/E3/DE/de/business/business/productivity/semi-autonomer-baustellenroboter-jaibot.html

Jenny, S. E., Pietrasik, L. L., Sounigo, E., Tsai, P., Gramazio, F., Kohler, M., Lloret-Fritschi, E., & Hutter, M. (2023). Continuous Mobile Thin-Layer On-Site printing. Automation in Construction, 146, 104634. https://doi.org/10.1016/j.autcon.2022.104634

Juricic, B. B., Galic, M., & Marenjak, S. (2021). Review of the construction labour demand and shortages in the EU. Buildings, 11(1), 17. https://doi.org/10.3390/buildings11010017

Kim, H., Hong, J., Song, E., Hong, T., & Choi, J. (2025). A multi-dimensional failure factor affecting the on-site adoption of construction robots. Developments in the Built Environment, 25, 100841. https://doi.org/10.1016/j.dibe.2025.100841

Knaack, U., Klein, T., Bilow, M., & Auer, T. (2007). Façades. Birkhäuser. https://doi.org/10.1007/978-3-7643-8281-0

Kolarevic, B. (2004). Architecture in the digital age. Taylor & Francis. https://doi.org/10.4324/9780203634561

Leschok, M., Cheibas, I., Piccioni, V., Seshadri, B., Schlüter, A., Gramazio, F., Kohler, M., & Dillenburger, B. (2023). 3D printing façades: Design, fabrication, and assessment methods. Automation in Construction, 152, 104918. https://doi.org/10.1016/j.autcon.2023.104918

McKinsey Global Institute. (2017). Reinventing construction: A route to higher productivity.

Meijs, M., & Knaack, U. (2009). Components and connections: Principles of Construction. Birkhäuser.

Melenbrink, N., Werfel, J., & Menges, A. (2020). On-site autonomous construction robots: Towards unsupervised building. Automation in Construction, 119, 103312. https://doi.org/10.1016/j.autcon.2020.103312

Minibuilders. (n.d.). https://robots.iaac.net/

Mitropoulou, I., Vaxman, A., Diamanti, O., & Dillenburger, B. (2024). Fabrication-aware strip-decomposable quadrilateral meshes. Computer-Aided Design, 168, 103666. https://doi.org/10.1016/j.cad.2023.103666

Mohsen, A. (2020). Li3-Method. In Mechanik, Werkstoffe und Konstruktion im Bauwesen (pp. 191–199). https://doi.org/10.1007/978-3-658-30204-7_6

MX3D. (2024, June 18). 3D printed smart Bridge in Amsterdam | MX3D. https://mx3d.com/industries/design/smart-bridge/

Nazir, A., Gokcekaya, O., Billah, K. M. M., Ertugrul, O., Jiang, J., Sun, J., & Hussain, S. (2023). Multi-material additive manufacturing: A systematic review of design, properties, applications, challenges, and 3D printing of materials and cellular metamaterials. Materials & Design, 226, 111661. https://doi.org/10.1016/j.matdes.2023.111661

Pajonk, A., Luna-Navarro, A., Knaack, U., & Blum, U. (2024). Additive manufacturing with varying material properties of thermosetting reactive polymers: A framework and comparison of different modes for implementing material transitions. Architectural Science Review, 1–13. https://doi.org/10.1080/00038628.2024.2348141

Pajonk, A., Prieto, A., Blum, U., & Knaack, U. (2022). Multi-material additive manufacturing in architecture and construction: A review. Journal of Building Engineering, 45, 103603. https://doi.org/10.1016/j.jobe.2021.103603

RAL-Gütegemeinschaft Fenster und Haustüren e.V. (2014). Leitfaden zur Planung und Ausführung der Montage von Fenstern und Haustüren für Neubau und Renovierung.

Rios, O., Carter, W., Post, B., Lloyd, P., Fenn, D., Kutchko, C., Rock, R., Olson, K., & Compton, B. (2018). 3D printing via ambient reactive extrusion. Materials Today Communications, 15, 333–336. https://doi.org/10.1016/j.mtcomm.2018.02.031

Robayo-Salazar, R., De Gutiérrez, R. M., Villaquirán-Caicedo, M. A., & Arjona, S. D. (2023). 3D printing with cementitious materials: Challenges and opportunities for the construction sector. Automation in Construction, 146, 104693. https://doi.org/10.1016/j.autcon.2022.104693

Robert McNeel & Associates. (n.d.). Rhinoceros 3D. https://www.rhino3d.com/

Romberg, S. K., Hershey, C. J., Lindahl, J. M., Carter, W. G., Condon, J., Kunc, V., & Compton, B. G. (2022). Large-scale reactive thermoset printing: Complex interactions between temperature evolution, viscosity, and cure shrinkage. The International Journal of Advanced Manufacturing Technology, 123(9–10), 3079–3094. https://doi.org/10.1007/s00170-022-10380-3

Saidi, K. S., Bock, T., & Georgoulas, C. (2016). Robotics in construction. In Springer Handbook of Robotics (2nd ed., pp. 1493–1520). Springer. https://doi.org/10.1007/978-3-319-32552-1_57

Sarakinioti, M. V., Turrin, M., Konstantinou, T., Tenpierik, M., & Knaack, U. (2018). Developing an integrated 3D-printed façade with complex geometries for active temperature control. Materials Today Communications, 15, 275–279. https://doi.org/10.1016/j.mtcomm.2018.02.027

Scorpion. (2024, June 26). Food4Rhino. https://www.food4rhino.com/en/app/scorpion

Stark, T., Binder, M., Bonfig, P., Hartwig, J., Jehl, W., Klos, H., Leuschner, I., Sieberath, U., & Sohn, E. (2016). Building Openings Construction Manual: Windows, Vents and Exterior Doors. Detail.

Strauss, H. (2012). AM Envelope. The potential of Additive Manufacturing for façade constructions. A+BE. https://doi.org/10.59490/abe.2013.1.477

Taseva, Y., Eftekhar, N., Kwon, H., Leschok, M., & Dillenburger, B. (2020). Large-Scale 3D printing for Functionally-Graded façade. Proceedings of the International Conference on Computer-Aided Architectural Design Research in Asia. https://doi.org/10.52842/conf.caadria.2020.1.183

Tenpierik, M., Turrin, M., Wattez, Y., Cosmatu, T., & Tsafou, S. (2018). Double Face 2.0: A lightweight translucent adaptable Trombe wall. SPOOL, 5(2). https://doi.org/10.7480/spool.2018.2.2090

Uitz, O., Koirala, P., Tehrani, M., & Seepersad, C. C. (2021). Fast, low-energy additive manufacturing of isotropic parts via reactive extrusion. Additive Manufacturing, 41, 101919. https://doi.org/10.1016/j.addma.2021.101919

Uitz, O., Leng, R., Pan, T., Zhao, X., Oridate, A., Seepersad, C., Ounaies, Z., & Frecker, M. (2023). Reactive extrusion additive manufacturing (REAM) of functionally graded, magneto-active thermoset composites. Additive Manufacturing, 67, 103486. https://doi.org/10.1016/j.addma.2023.103486

Universal Robots A/S. (2016). UR5 Technical specifications. https://www.universal-robots.com/media/50588/ur5_en.pdf

ViscoTec Pumpen- u. Dosiertechnik GmbH. (2024, June 21). 3D Print Heads. https://www.viscotec.de/en/products/3d-print-heads/

Visose. (n.d.). GitHub - visose/Robots: Create and simulate ABB, KUKA, UR, and Staubli robot programs. GitHub. https://github.com/visose/Robots

VHV-Bauschadenbericht. (2022). Hochbau 2021/22. Fraunhofer, Stuttgart.

Wang, T., Mao, C., Sun, B., & Li, Z. (2024). Genealogy of construction robotics. Automation in Construction, 166, 105607. https://doi.org/10.1016/j.autcon.2024.105607

Wiscombe, T. (2012). Beyond assemblies: System convergence and multi-materiality. Bioinspiration & Biomimetics, 7(1), 015001. https://doi.org/10.1088/1748-3182/7/1/015001

Wolf, A., Rosendahl, P. L., & Knaack, U. (2022). Additive manufacturing of clay and ceramic building components. Automation in Construction, 133, 103956. https://doi.org/10.1016/j.autcon.2021.103956

Wynne, Z., Buchanan, C., Kyvelou, P., Gardner, L., Kromanis, R., Stratford, T., & Reynolds, T. P. S. (2022). Dynamic testing and analysis of the world's first metal 3D printed bridge. Case Studies in Construction Materials, 17, e01541. https://doi.org/10.1016/j.cscm.2022.e01541

XtreeE. (n.d.). XtreeE | The large-scale 3D. https://xtreee.com/en/

Zuo, Z., De Corte, W., Huang, Y., Chen, X., Zhang, Y., Li, J., Zhang, L., Xiao, J., Yuan, Y., Zhang, K., Zhang, L., & Mechtcherine, V. (2023). Propelling the widespread adoption of large-scale 3D printing. Nature Reviews Materials. https://doi.org/10.1038/s41578-023-00626-1